Original Articles

Acupuncture and Herbal Medicine

Daphnegiravone D synergistically inhibits liver cancer in combination with oxaliplatin *in vitro* and *in vivo*

Yu-Jue Wang[1,2,3,4], Jiao-Yang Hou[1,2,3,4], Xin-Ye Wang[1,2,3,4], Hong-Fei Chen[1,2,3,4], Shuang Qiu[1,2,3,4], Qing-Bo Liu[1,2,3,4], Xiao-Xiao Huang[1,2,3,4], Guo-Dong Yao[1,2,3,4,*], Shao-Jiang Song[1,2,3,4,*]

[1]Key Laboratory of Computational Chemistry-Based Natural Antitumor Drug Research & Development, Shenyang Pharmaceutical University, Shenyang, China; [2]School of Traditional Chinese Materia Medica, Shenyang Pharmaceutical University, Shenyang, China; [3]Engineering Research Center of Natural Medicine Active Molecule Research & Development, Liaoning, Shenyang Pharmaceutical University, Shenyang, China; [4]Key Laboratory of Natural Bioactive Compounds Discovery & Modification, Shenyang, Shenyang Pharmaceutical University, Shenyang, China

Abstract

Objective: Daphnegiravone D (DGD), a prenylated flavonoid from *Daphne giraldii* Nitsche, a plant whose roots and stem are used in Chinese medicine, exerts an inhibitory effect on liver cancer cells. The protein kinase ataxia telangiectasia-mutated and Rad3-related (ATR) is an important component of the DNA damage response, and its inhibition enhances the sensitivity of some cancer cells to DNA-damaging drugs. Oxaliplatin (OXA) is a third-generation, platinum-based anticancer drug that exerts its inhibitory effects on liver cancer cells by inhibiting DNA synthesis. Owing to the fact that most patients develop drug resistance, finding novel treatments for liver cancer is urgent. In a previous study, DGD was shown to exert anti-tumor effects as a potential ATR kinase inhibitor. This study investigated the mechanism of action of DGD and its combination with OXA in liver cancer.

Methods: HepG2 and Hep3B cells were used to evaluate the inhibitory effects of DGD on liver cancer. Cellular thermal shift assay, co-immunoprecipitation, and western blotting were used to confirm the impact of DGD on DNA damage. The methyl thiazolyl tetrazolium (MTT) assay was performed, and the resulting data were used to calculate drug synergy scores. Acridine orange/ethidium bromide staining, Annexin V/propidium iodide staining, reactive oxygen species–related staining, and western blotting were performed to assess the efficacy of the combination of DGD and OXA. An *in vivo* tumor xenograft model in nude mice was used to investigate the efficacy of this combination. Hematoxylin–eosin staining and immunohistochemistry were performed to observe the condition of tissues *in vivo*.

Results: DGD inhibited liver cancer cells by affecting the formation of the ATR-ATRIP complex and downregulating the activator protein TopBP1. We found that DGD and OXA showed synergistic growth-inhibitory effects in liver cancer cells *in vitro*. DGD and OXA showed synergistic growth-inhibitory effects in liver cancer cells *in vitro* and showed lower cytotoxicity toward L-02 cells than an equi-effective higher concentration of OXA under the tested conditions in normal liver cells. The combination was associated with enhanced apoptosis, mitochondrial dysfunction, and oxidative stress. Further experiments suggested that DGD may enhance OXA-induced DNA damage, at least partly in association with suppression of ATR-related signaling. Consistent with the above results, DGD enhanced the antitumor efficacy of OXA *in vivo* without causing overt additional toxicity under the present experimental conditions.

Conclusion: Our findings indicate that DGD enhances the antitumor activity of OXA against liver cancer, with the *in vitro* synergistic effect being associated, at least partly, with suppression of ATR-related signaling, enhanced DNA damage, and oxidative stress. DGD also improved the antitumor efficacy of OXA in the xenograft model without overt additional toxicity.

Keywords: ATR, Daphnegiravone D, Drug combination, Liver cancer, Oxaliplatin

Introduction

Liver cancer remains one of the most lethal malignancies worldwide, with rising incidence and mortality rates, and a particularly poor 5-year survival rate among patients with advanced disease[1–2]. As a third-generation platinum-based agent, oxaliplatin (OXA) exerts anti-tumor effects primarily by inducing DNA inter- and intra-strand crosslinking, which results in DNA damage[3–4]. Therefore, OXA-based chemotherapeutic drugs, used alone or in combination with other

Yu-Jue Wang and Jiao-Yang Hou contributed equally to this work.

**Corresponding author. Guo-Dong Yao, E-mail: guodong_yao@syphu.edu.cn; Shao-Jiang Song, E-mail: 103050102@syphu.edu.cn.*

How to cite this article: Wang YJ, Hou JY, Wang XY, Chen HF, Qiu S, Liu QB, Huang XX, Yao GD, Song SJ. Daphnegiravone D synergistically inhibits liver cancer in combination with oxaliplatin in vitro and in vivo. Acupunct Herb Med 2026;6(3):372–386. doi: 10.1097/HM9.0000000000000201

Received 22 October 2025 / Accepted 26 April 2026

Copyright © 2026 Tianjin University of Traditional Chinese Medicine. This is an open-access article distributed under the terms of the Creative Commons Attribution-Non Commercial-No Derivatives License 4.0 (CCBY-NC-ND), where it is permissible to download and share the work provided it is properly cited. The work cannot be changed in any way or used commercially without permission from the journal.

HM9_V6N3.indb 372 26-Sep-26 15:38:16

agents, represent a treatment option for patients with advanced liver cancer[5–6]. However, its clinical efficacy is often limited by side effects[7]. In recent years, natural products have become a major source of therapeutic and preventive agents against various diseases, including cancer[8]. Among phytopharmaceuticals, flavonoids including quercetin, kaempferol, and luteolin have been shown not only to enhance the anti-tumor activity of chemotherapy drugs but also to reduce their toxic side effects[9–11]. Therefore, the combination of suitable natural products with conventional chemotherapeutic agents holds significant promise for the treatment of liver cancer.

Daphne giraldii Nitsche is a member of the Thymelaeaceae family, whose roots and stems are used as medicine, called *ZuShiMa*. In a previous study, it was found that Daphnegiravone D (DGD), a prenylated flavonoid from *D. giraldii* Nitsche, inhibits liver cancer cells by inhibiting ataxia telangiectasia and Rad3-related (ATR) kinase[12].

ATR is a key protein kinase in the DNA damage response, and regulates downstream factors to arrest the cell cycle, stabilize replication forks, and promote DNA repair, thereby suppressing apoptosis[13–15]. In cancer cells, defects in the acquired DNA damage response promote cell proliferation, tumorigenesis, and tumor progression. Moreover, chemotherapy insensitivity is often linked to dysregulated DNA damage response pathways[16–18]. Given the central role of ATR in DNA damage response signaling, ATR inhibitors hold substantial therapeutic potential to improve oncological outcomes, either as monotherapy or in combination with DNA-damaging chemotherapeutic agents, ionizing radiation (IR), immune checkpoint blockers, or poly ADP-Ribose polymerase inhibitors[19–21]. Therefore, this study aimed to investigate the underlying molecular mechanism by which DGD enhances the anti-liver cancer effects of OXA.

Materials and methods

Chemicals and reagents

DGD (purity ≥98%) was isolated from *D. giraldii* in our laboratory, with a molecular formula of $C_{26}H_{28}O_6$[22]. OXA (S1224) was purchased from Selleck Chemicals (Houston, Texas, USA). Furthermore, 3-(4,5-dimethylthiazol-2-yl)-2,5-diphenyltetrazolium bromide (MTT, M2128) was purchased from Sigma-Aldrich Co., Ltd. (St. Louis, Missouri, USA). Fetal bovine serum (FBS) was purchased from Zhejiang Tianhang Biotechnology Co., Ltd. (Hangzhou, China). Dulbecco's modified Eagle's medium (DMEM), phosphate-buffered saline (PBS), and antibiotics (100 U/mL penicillin, 100 μg/mL streptomycin) were purchased from HyClone, Inc. (Logan, Utah, USA). Dichlorofluorescein diacetate (H_2DCF-DA, S1105S), Hoechst 33258 (C1011), JC-1 (C2005), NP-40 lysis buffer (P0013F), radioimmunoprecipitation assay lysis buffer (P0013B), commercial caspase-3 assay kits (C1073S), and BCA assay kits (P0009) were purchased from Beyotime (Shanghai, China). Annexin V-fluorescein isothiocyanate (FITC) and propidium iodide (PI) were purchased from Bimake (Houston, TX, USA). Polyvinylidene fluoride (PVDF) membranes (0.2 μm) were purchased from Millipore (Middlesex, Massachusetts, USA). MitoSOX™ Red mitochondrial superoxide indicator was purchased from Molecular Probes (Eugene, Oregon, USA). Antibodies against Bax, Bcl-xl (sc-8392), p38 (sc-7149), and β-actin (sc-58673) were purchased from Santa Cruz Biotechnology Inc. (Santa Cruz, CA, USA). Antibodies against ATR (13934), ATRIP (97687), p-CHK1 (Ser345) (2348), γ-H_2AX (Ser139) (2577), and p-p38 MAPK (Thr180/Tyr182) (4511) were purchased from Cell Signaling Technology (Danvers, Massachusetts, USA). Antibodies against TopBP1 (23340-1-AP) were purchased from Proteintech (Rosemount, IL, USA). Horseradish peroxidase-conjugated secondary antibodies (goat anti-rabbit or goat anti-mouse) were purchased from Santa Cruz Biotechnology (Santa Cruz, CA, USA).

Cell culture

Hep3B and HepG2 cells were used as the liver cancer cell lines. L-02 cells were used as normal human liver cells. Hep3B and HepG2 cells were obtained from the American Type Culture Collection (Manassas, VA, USA). L-02 cells were obtained from the National Collection of Authenticated Cell Cultures (Shanghai, China). The cells were cultured in DMEM supplemented with 10% FBS and 1% antibiotics. Cells were incubated at 37°C with 5% CO_2 in a humidified atmosphere. All the experiments were performed using cells grown logarithmically.

Cellular thermal shift assay

Cellular thermal shift assay (CETSA) was performed on cell lysates and intact cells. For CETSA of Hep3B and HepG2 cell lysates, the cells were lysed with lysis buffer supplemented with a protease inhibitor cocktail. After centrifugation, the supernatant was aspirated into a new tube, incubated with dimethyl sulfoxide or DGD for 1 hour at room temperature, and heated for 3 minutes in a polymerase chain reaction (PCR) machine. The heated lysates were centrifuged to separate the precipitated proteins from the soluble fractions. Finally, the supernatant was loaded onto a sodium dodecyl sulfate-polyacrylamide gel electrophoresis (SDS-PAGE) gel and subjected to immunoblotting.

Cell proliferative assay

Cells were seeded in 96-well plates at a density of 5×10^3 cells/well before the addition of DGD, OXA, or their combination. After incubation for 48 hours, MTT (5 mg/mL) was added. The absorbance of the plates was measured at 450 nm using a microplate reader (Molecular Devices; Thermo, Waltham, Massachusetts, USA). The SynergyFinder on-line software was used to calculate drug synergy scores with the "inhibition index" by the response surface model and zero interaction potency (ZIP) calculation method. ZIP synergy scores greater than 10 were considered strongly synergistic, and the gradation of the red regions indicated the intensity of the synergism[23–24].

HM9_V6N3.indb 373 26-Sep-26 15:38:16

Western blot analysis

Cells were seeded in 6-well plates at a density of 2×10^5 cells/well for 48 hours before adding DGD, OXA, or their combination. After treatment, the Hep3B and HepG2 cells were harvested and washed with PBS. Total cellular protein was isolated using protein extraction buffer and quantified using the BCA protein assay kit. Cell lysates in 5× SDS sample buffer were boiled for 10 minutes. Subsequently, equal amounts of protein were fractionated using 8% to 12% SDS-PAGE and transferred to PVDF membranes. After blocking with phosphate-buffered saline with Tween-20 (PBST) containing 5% dried skimmed milk, the membranes were incubated with primary antibodies at 4°C overnight. After washing with PBS, the blots were incubated with the corresponding horseradish peroxidase–conjugated goat anti-mouse or anti-rabbit secondary antibodies, followed by detection using ECL Plus reagent.

Co-immunoprecipitation assays

Hep3B and HepG2 cells were inoculated in 10 cm Petri dishes and treated with different concentrations of DGD or vehicle as a control. Subsequently, 40 µL protein A/G magnetic beads (purchased from Bimake, Houston, Texas, USA) were incubated with an anti-ATR or anti-ATRIP antibody at room temperature for 2 hours. Subsequently, the supernatant was aspirated and the prepared cell lysate was added for further rotation at room temperature for 1 hour. The beads were washed three times with lysis buffer, and the immune complexes were eluted at 95°C for 5 minutes with 5× loading buffer. The complexes were separated by SDS-PAGE and subjected to Western blot analysis.

Apoptosis assay

Notably, Hep3B and HepG2 cells were each seeded at 2.5 x 10^5 cells per well in six-well plates, and after 12 hours, DGD, OXA, or a combination of both were added, and the plates were incubated for 48 hours. Cell apoptosis was evaluated using the Annexin V-FITC/PI apoptosis detection kit. Following the manufacturer's instructions, analysis was performed by flow cytometry and quantified using FlowJO software. Apoptosis was detected using AO/EB and Hoechst 33258 staining. After incubation, nuclear morphology was observed and photographed under different fluorescence wavelengths using a fluorescence microscope. In addition, a phase-contrast microscope was used to observe the cell morphology.

Quantification of caspase-3 activities

Caspase-3 kits were used to quantify the caspase activity. HepG2 and Hep3B cells were seeded in six-well plates and exposed to indicated concentrations of DGD, OXA, or their combination. After 48 hours of treatment, the cells were collected and analyzed according to the manufacturer's protocol, after which the absorbance values were measured using a microplate reader at a wavelength of 405 nm. Caspase-3 activity is expressed as a percentage of the control.

Examination of mitochondrial function and oxidative stress

Hep3B and HepG2 cells were seeded in a six-well plate and treated with different doses of DGD and OXA, either alone or in combination. The cells were stained with 2',7'-dichlorodihydrofluorescein diacetate (DCFH-DA) for general intracellular reactive oxygen species (ROS) levels in the dark at 37°C for 30 minutes. MitoSOX staining was used to detect the level of superoxide anion in mitochondria at 37°C for 10 minutes in the dark. JC-1 was used to measure the loss of mitochondrial membrane potential (MMP) at 37°C for 20 minutes in the dark. Dihydroethidium (DHE), ROS Green H_2O_2, hydroxyphenyl fluorescein (HPF), and C11-BODIPY 581/591 probe were used to detect different reactive oxygen species and lipid peroxidation superoxide substances. After 10 minutes of incubation at 37°C, the samples were rinsed twice with PBS. Subsequently, the generation of intracellular superoxide, H_2O_2, ·OH, and lipid peroxides was examined sequentially by fluorescence microscopy.

Real-time PCR

RNA was extracted from Hep3B and HepG2 cells subjected to various treatments using TRIzol reagent, and the concentration and purity were measured. A Revert Aid First Strand cDNA Synthesis Kit (TaKaRa, Shiga, Japan) was used to synthesize cDNA by reverse transcription. The mRNA expression levels were evaluated by real-time PCR according to the manufacturer's instructions. The primer sequences used were as follows:

ATR, forward primer, 5'- CTATGGGAACAGAGGGT CTTTT-3', reverse primer, 5'-TGGTTTACTCCATTCCAC AAGA-3';

ATRIP, forward primer, 5'-TGCCACCTCCTGAGTAG TAGTTCTG-3', reverse primer, 5'-ATTCCAGCCAAGGT ACTGCCAAAC-3';

TopBP1, forward primer, 5'-CCAGAAATGACAAAG AACCGTT-3', reverse primer, 5'-TCAAAGACAACGC CACTAAAAG-3';

CHK1, forward primer, 5'-CTCAAGTTTTGGCGG GAAAAG-3', reverse primer, 5'- AAGTTGAACTTCTC CATAGGCA-3';

In vivo anti-tumor activity

Male BALB/c athymic nude mice (4 weeks of age and weighing approximately 20 g) were purchased from Beijing Huafukang Biotechnology Co., Ltd. (Beijing, China) and maintained under standard pathogen-free conditions in the Experimental Animal Center of Shenyang Pharmaceutical University. Mice were allowed to acclimatize for 7 days after arrival before any experimental procedures, with free access to food and water. Mice were housed in individually ventilated cages under a 12 h light/dark cycle, at 25°C and 55% relative humidity. Animal care and experimental protocols were performed in accordance with the guidelines established by the Shenyang Pharmaceutical University Institutional Animal Care and Use Committee (ethical approval number: SYPU-IACUC-S2022-10.19-101).

Hep3B cells (1×10^7 cells) were subcutaneously injected into the right flank of each mouse. Mice were randomly

HM9_V6N3.indb 374 26-Sep-26 15:38:16

assigned to different treatment groups using a random number generator after tumor volume reached 100 mm^3. Animals were randomly allocated to treatment groups after tumor establishment using a computer-generated randomization sequence. Tumor measurements,histological evaluation and image quantification were performed by investigators blinded to group allocation until the analysis was completed. The mice were randomly divided into control, DGD, OXA, and DGD-OXA combination groups, 5 each group. The control group was treated with 0.1 mL 5% glucose solution every 2 days. The DGD group was treated with 0.1 mL 5 mg/kg DGD intraperitoneally every 2 days. The OXA group was treated with 0.1 mL 5 mg/kg OXA intraperitoneally every 2 days. The DGD-OXA combination group was treated with 0.1 mL DGD (5 mg/kg) plus 0.1 mL OXA (5 mg/kg) intraperitoneally every 2 days. Tumor growth and mouse weight measurement were done by investigators unknown to group assignment. Animal cages were identified only by number, coded until unblinding after data analysis was completed. Tumor growth and mouse weight were evaluated daily, and tumor volume was calculated using the following formula: $V = L \times W^2 \times 0.5236$, where V is the volume, L is the length, and W is the width. Tumor growth and body-weight data were analyzed using two-way ANOVA. Animals were monitored daily for body weight, activity, posture, grooming, food and water intake, and signs of pain or distress. No pre-specified humane-endpoint criteria were recorded in the available experimental documentation. The animals were euthanised at the end of the planned experiment or earlier if severe clinical deterioration occurred, in accordance with the approved institutional protocol. Anaesthesia and euthanasia were performed using isoflurane inhalation anaesthesia followed by cervical dislocation, respectively, in accordance with the approved institutional animal-use protocol. The mice were euthanised after 2 weeks, after which the tumors and major organs were immediately collected for histological and immunohistochemical analysis.

Histopathological and immunohistochemical examinations

The major mouse organs were embedded in paraffin, cut into 4-μm sections, stained with hematoxylin and eosin, and then observed under a light microscope for the evaluation of the potential toxicity of the drug to the organ. For immunohistochemical staining, tumor tissues were embedded in paraffin and cut into 4-μm slices. Subsequently, the paraffin-embedded tumor sections were deparaffinized, rehydrated, and subjected to antigen retrieval. Next, sections were incubated with primary antibodies against ATR and Ki67 overnight at 4°C. After incubation with secondary antibodies, the tissue morphology of the sections was analyzed under a microscope.

Statistical analysis

All data were analyzed using GraphPad Prism 9.0 (GraphPad Software, Boston, Massachusetts, USA). Biological replicates were set up for all experiments. Every experiment was performed at least three times (the specific number of replicates was indicated in each figure legend), and the results are expressed as mean ± standard deviation (SD). Data normality was assessed using the Shapiro-Wilk test. For two-group comparisons, an unpaired two-tailed Student t test was used. For multi-group comparisons, one- or two-way analysis of variance (ANOVA) was performed followed by Tukey's post hoc test. Nonparametric tests were applied for non-normally distributed data: the Mann-Whitney U test for two-group comparisons and the Kruskal-Wallis test with Dunn's post hoc analysis for three or more groups. For multiple measurements from the same mouse, two-way repeated-measures ANOVA with a single pooled variance was used, applying Tukey's correction for data normality within groups. P values of <0.05 were considered statistically significant.

Results

DGD affects ATR–ATRIP complex formation in liver cancer cells

As the first step in exploring how DGD targets ATR to inhibit liver cancer cells, its suppressive effect on liver cancer cells was investigated. DGD exhibited potent cytotoxicity in a concentration-dependent manner against HepG2 and Hep3B cells with 50% inhibitory concentration (IC_{50}) values of 7.78 ± 0.89 and 1.68 ± 0.48 μM, respectively, and no obvious effect on normal human hepatic cells (L-02 cells) (Figure 1A). Next, we explored the ability of DGD to bind ATR. The CETSA results supported cellular target engagement between DGD and ATR (Figure 1B). DGD showed a good binding affinity with ATR (PDB ID:9L43) through molecular docking, with a docking score of –8.6 (Figure 1C). These docking results suggest a potential interaction between DGD and ATR.

On DNA damage from either endogenous or exogenous sources, ATR is recruited to the damaged site, where it binds to the ATR-interacting protein (ATRIP) to form a complex[25]. This ATR–ATRIP complex undergoes a conformational change upon interaction with topoisomerase II-binding protein 1 (TopBP1), leading to the phosphorylation of the downstream checkpoint kinase CHK1 and ultimately promoting cell survival[26–28]. Therefore, a co-immunoprecipitation (Co-IP) assay was used to measure the effect of DGD on ATR–ATRIP complex formation. The results suggested that DGD inhibited the interaction between ATR and ATRIP in a concentration-dependent manner (Figure 2A, B). Western blotting revealed significant downregulation of TopBP1 protein expression upon DGD treatment, with a concomitant reduction in CHK1 phosphorylation (Figure 2C, D). Taken together, these data indicate that DGD may inhibit the recruitment of the activator TopBP1 and its downstream regulators by affecting the stability of the ATR–ATRIP complex, thereby limiting the adequate activation of ATR in DNA damage response.

DGD promotes OXA-induced apoptosis in liver cancer cells

ATR inhibition sensitizes cancer cells to DNA-damaging agents and IR[29–30]. Accordingly, ATR inhibitors are frequently combined with DNA-damaging chemotherapeutics in clinical settings to improve treatment outcomes[31–32]. Given that earlier data indicated that DGD may act as a modulator of ATR-related signaling in liver cancer, we investigated whether it could enhance the efficacy of

HM9_V6N3.indb 375 26-Sep-26 15:38:16

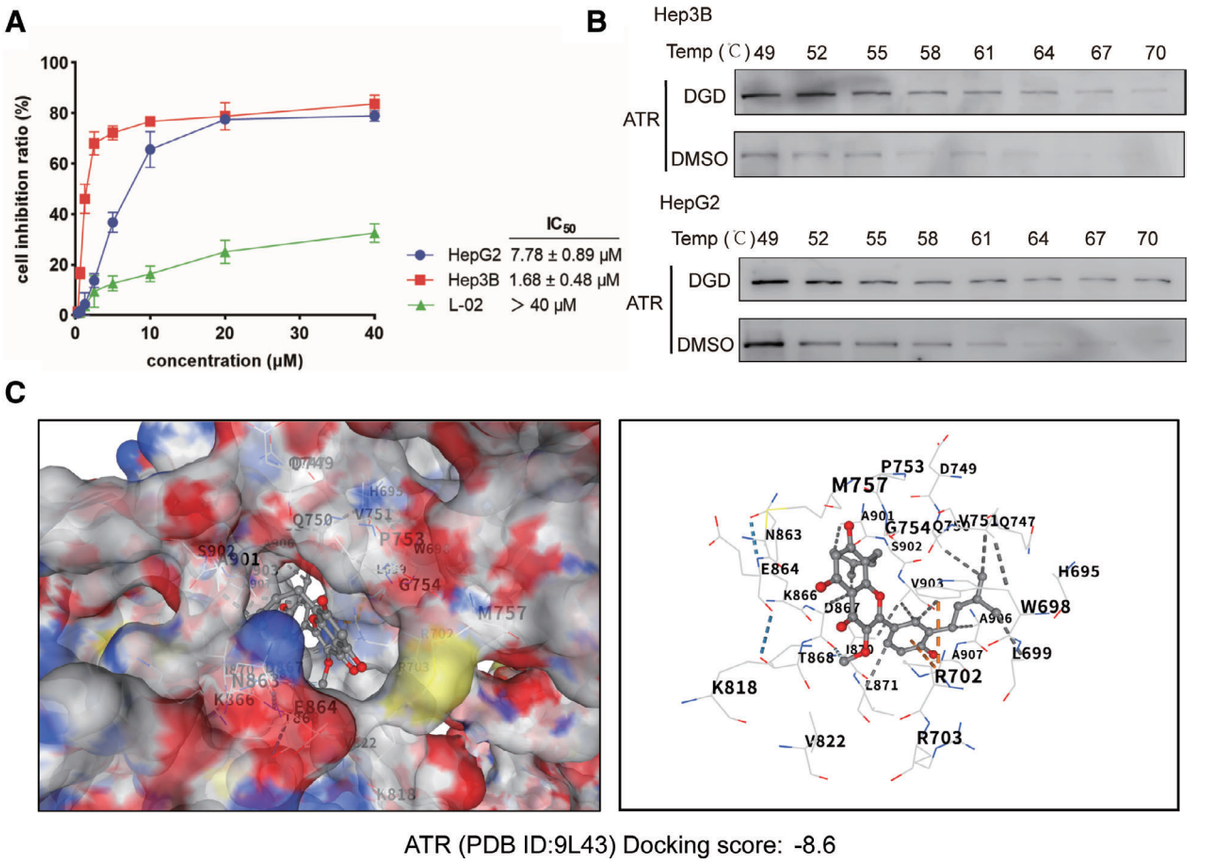


Figure 1. ATR is a target for DGD to exert anti-tumor effects. (A) Cytotoxicity after treatment with various DGD concentrations in HepG2, Hep3B, and L-02 cells for 48 h. The data are presented as the mean ± SD of three independent experiments. (B) The stabilization effect of DGD on ATR at different temperatures was assessed *via* cellular thermal shift assay ($n = 3$). (C) The molecular docking and docking score of DGD with ATR. ATR: Ataxia telangiectasia and Rad3-related kinase; DGD: Daphnegiravone D; DMSO: Dimethyl sulfoxide; IC_{50}: 50% inhibitory concentration; SD: Standard deviation.

chemotherapy. To evaluate the combined effect, liver cancer cells were co-treated with DGD and OXA. Cell viability was assessed using the MTT assay, and drug ZIP synergy scores were calculated using the SynergyFinder on-line software. As shown in Figure 3A and B, the average ZIP scores indicated a significantly strong synergistic anti-tumor effect in the majority of the DGD-OXA combination treatments (ZIP synergy scores >10 indicated synergism). The combination index (CI) values of the combination of DGD and OXA (1:1) in Hep3B and HepG2 cells were determined using CalcuSyn2.1 software. At low concentrations, the combination therapy showed better inhibitory effects than monotherapy (CI <1) (Figure 3C). When 50% of the liver cancer cells were inhibited, the CI values were all <1, indicating a good synergistic effect (Figure 3D). In addition, we observed that OXA (4.5 μM) and DGD (6 μM) had the same inhibitory effect on HepG2 cells as 10 μM OXA, and the toxicity to L-02 was significantly decreased compared with 10 μM OXA (Figure 3E). The combination therapy significantly reduced OXA-induced toxicity.

OXA-induced apoptosis is an important mechanism underlying its anti-tumor effects. Phase-contrast microscopy was used to observe morphological changes in liver cancer cells. As shown in Figure 4A, the treated cells presented the typical morphology of apoptotic cells, such as rounding and wrinkling. Hoechst 33258 and AO/EB staining demonstrated that combination treatment significantly increased chromatin condensation and nuclear fragmentation (Figure 4A). Furthermore, flow cytometry revealed that DGD combined with OXA markedly induced apoptosis compared to the untreated cells and the single-drug group (Figure 4B). Caspase-3 is the most frequently activated death protease during the early stages of apoptosis, and is an important marker of apoptosis[33]. Therefore, apoptosis triggered by OXA and DGD was further confirmed by the detection of caspase-3 activity and western blot analysis of Hep3B and HepG2 cells. The results showed that the DGD-OXA combination enhanced caspase-3 activity and the expression of the pro-apoptotic protein Bax, while the combination reduced the expression of the anti-apoptotic protein Bcl-xl (Figure 2C–E). In summary, the combination of DGD and OXA synergistically induces apoptosis in liver cancer cells.

DGD combined with OXA enhanced mitochondrial damage and oxidative stress in liver cancer cells

OXA exerts its inhibitory effect on tumor cells by accumulating in the mitochondria and inducing oxidative stress, resulting in excessive ROS production[34–35]. Therefore, we used a JC-1 fluorescent probe to detect changes in MMP. DGD combined with OXA significantly reduced

HM9_V6N3.indb 376 26-Sep-26 15:38:17

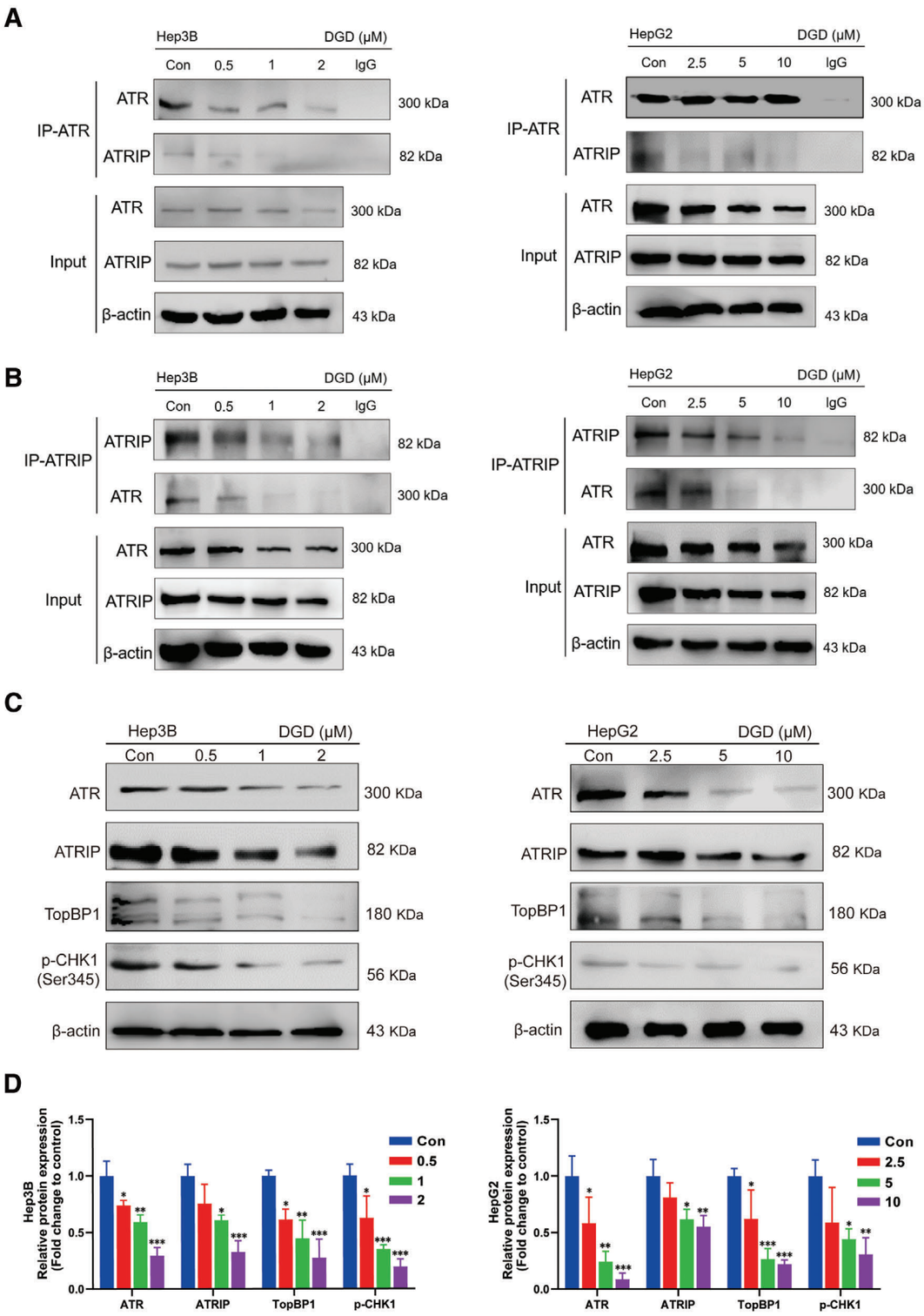


Figure 2. Effect of DGD on the ATRIP complex in liver cancer cells. (A, B) Co-immunoprecipitation analysis of the effect of DGD on the ATR–ATRIP complex ($n = 3$). (C, D) western blotting was performed to detect the levels of ATR, ATRIP, TopBP1, and p-CHK1 in different treatment groups ($n = 3$). *$P < 0.05$, **$P < 0.01$, ***$P < 0.001$ *vs.* control group. ATR: Ataxia telangiectasia and Rad3-related kinase; ATRIP: ATR-ATR-interacting protein; DGD: Daphnegiravone D.

MMP compared to the drug-only group. To examine the level of superoxide in the mitochondria, the fluorescent probe MitoSOX™ Red was used, and red fluorescence was found to be strongly enhanced in the co-administration group (Figure 5A).

Oxidative stress results from an imbalance between ROS generation and the antioxidant defense systems. It has been found to be associated with DNA damage and apoptosis induction[36–37]. Therefore, we measured the intracellular ROS levels using the oxidation-sensitive

HM9_V6N3.indb 377 26-Sep-26 15:38:18

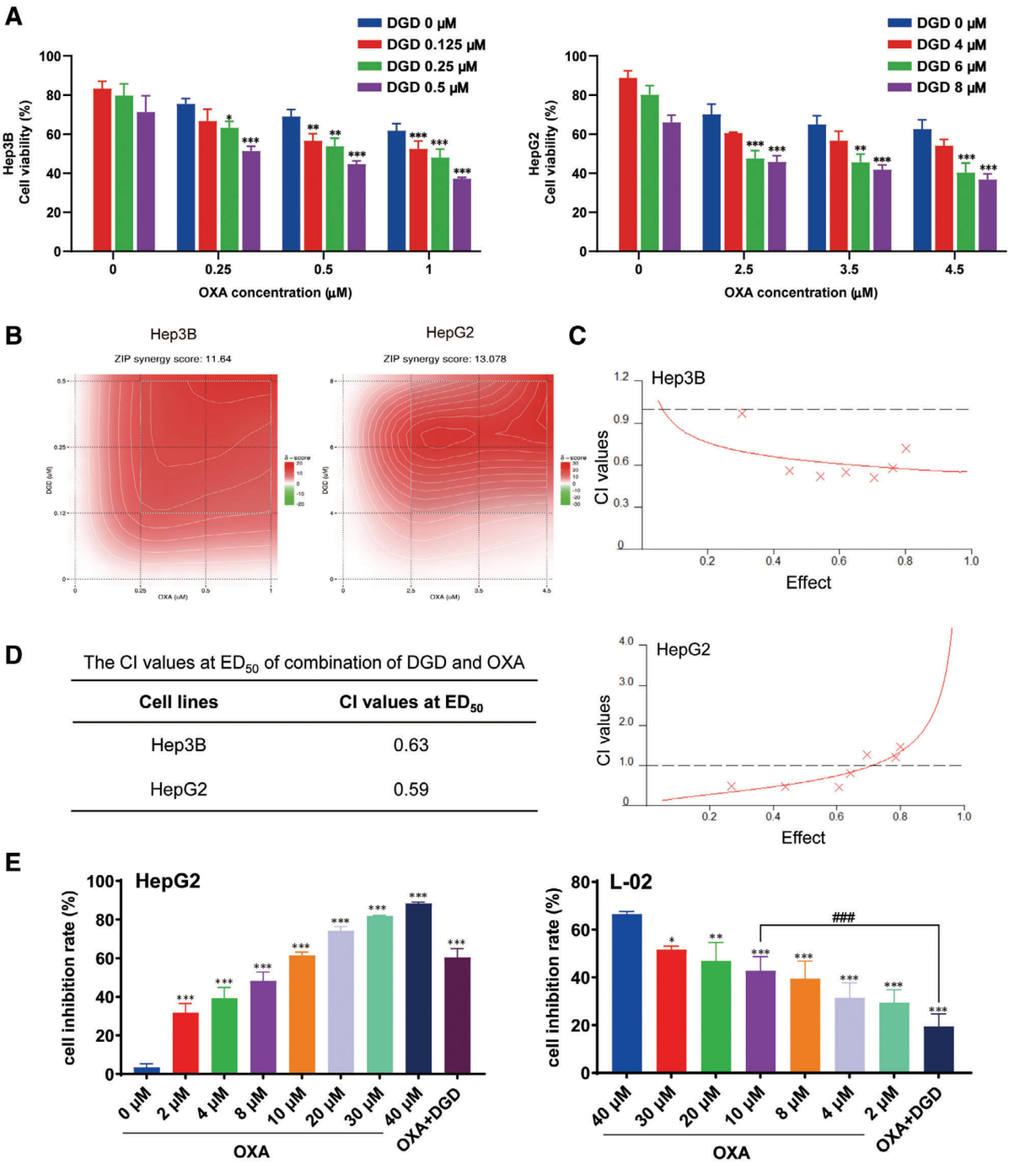


Figure 3. Combined effects of DGD and OXA on liver cancer. (A) Combined cytotoxicity after treatment with various concentrations of DGD and OXA for 48 h. (B) ZIP synergy plot of the drug combination responses. (C) CI values of the combination of DGD and OXA in liver cancer cells using CalcuSyn software. (D) CI values at ED_{50} of DGD and OXA. (E) Cytotoxicity after treatment with combined OXA (4.5 μM) with DGD (6 μM) and various OXA concentrations in HepG2 and L-02 cells for 48 h. The data are presented as the mean ± SD of three independent experiments. *$P < 0.05$, **$P < 0.01$, ***$P < 0.001$ *vs*. 0 μM group in HepG2 or 40 μM group in L-02, ###$P < 0.001$ *vs*. OXA 10 μM group. CI: Combination index; DGD: Daphnegiravone D; ED_{50}: Median effective dose; OXA: Oxaliplatin; SD: Standard deviation; ZIP: Zero interaction potency.

fluorescent probe H_2DCF-DA (Figure 5B). Flow cytometry and staining results showed that cells co-treated with DGD and OXA exhibited significantly increased ROS production. Moreover, based on the results of DHE, ROSGreen H_2O_2, and HPF fluorescence staining, DGD and OXA co-treatment increased the accumulation of superoxide anions (O_2^-), hydrogen peroxide (H_2O_2), and hydroxyl radicals (·OH), respectively. DGD in combination with OXA substantially elevated intracellular lipid peroxidation levels, as assessed by C11 BODIPY 581/591 staining (Figure 5C). In addition, the inhibitory effects of DGD, OXA alone, and DGD–OXA combination on liver cancer cells were reversed after N-acetyl-L-cysteine (NAC) treatment (Figure 5D). These results suggest that

HM9_V6N3.indb 378 26-Sep-26 15:38:19

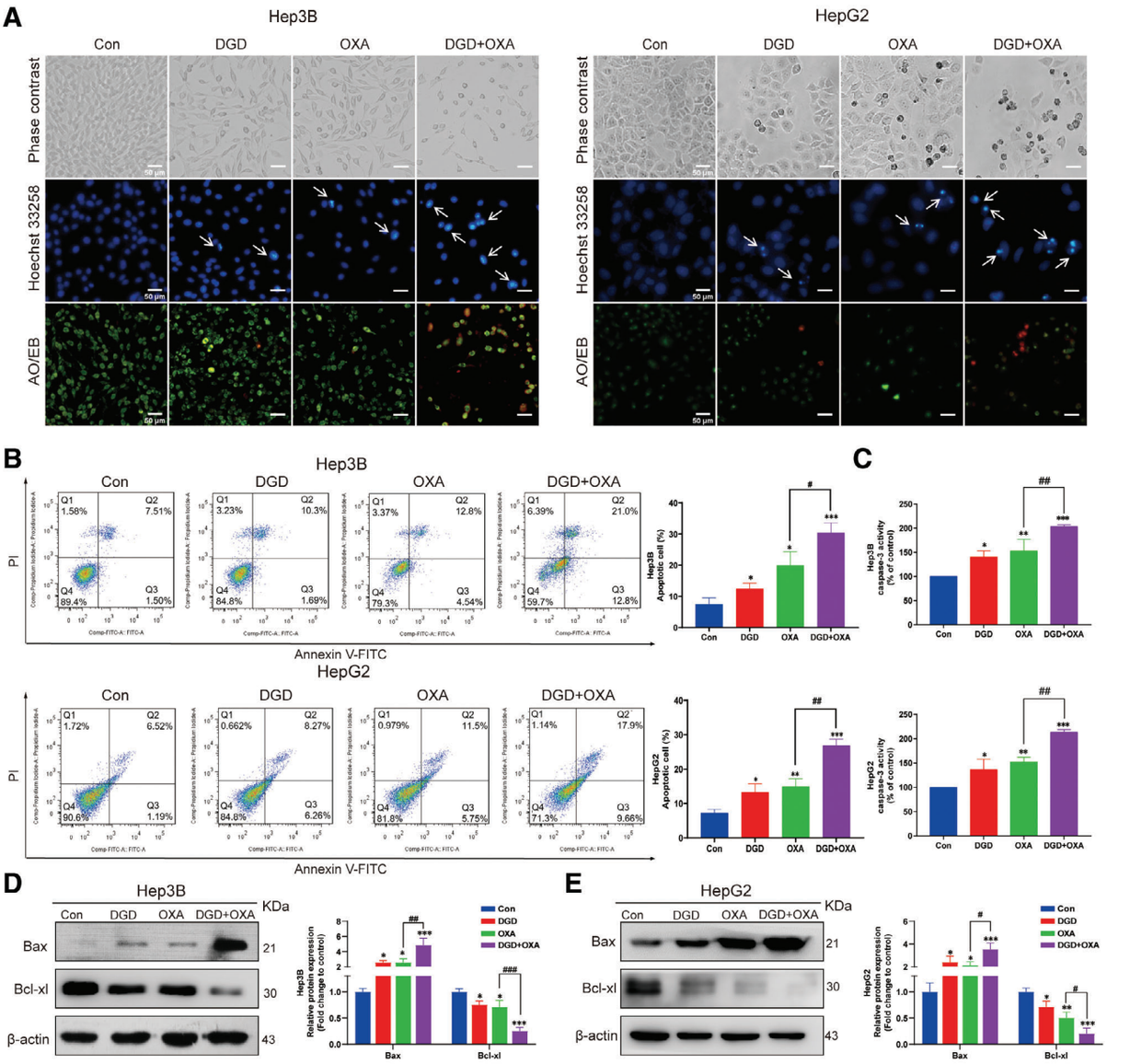


Figure 4. DGD and OXA synergistically induce apoptosis in liver cancer cells. (A) Phase-contrast microscopy and Hoechst 33258 and AO/EB staining were used to detect the effects of DGD and OXA alone or in combination on apoptosis in Hep3B (DGD = 0.5 μM, OXA = 1 μM) and HepG2 (DGD = 6 μM, OXA = 4.5 μM) cells for 48 h ($n = 3$). White arrows indicate apoptotic cells. Scale bar represents 50 μm. (B) Hep3B and HepG2 cells were stained with Annexin V-FITC and PI probes to estimate cell apoptosis using flow cytometry ($n = 3$). (C) Caspase-3 activity was detected using a caspase-3 kit assay in Hep3B and HepG2 cells ($n = 3$). (D, E) Protein expression levels of Bax and Bcl-xl in Hep3B and HepG2 cells were estimated by western blotting ($n = 3$). The data are presented as the means ± SD of three independent experiments (*$P < 0.05$, **$P < 0.01$, ***$P < 0.001$ *vs*. control, $^{\#}P < 0.05$, $^{\#\#}P < 0.01$, $^{\#\#\#}P < 0.001$ *vs*. OXA group). DGD: Daphnegiravone D; FITC: Fluorescein isothiocyanate; OXA: Oxaliplatin; PI: Propidium iodide; SD: Standard deviation.

DGD enhances OXA-induced mitochondrial damage and oxidative stress in liver cancer cells.

DGD increased OXA sensitivity in association with suppression of ATR-related signaling

To decipher the mechanism by which DGD synergizes with OXA, western blotting was performed to detect the expression of ATR-related proteins in liver cancer cells. Our results showed that the expression levels of ATR, ATRIP, TopBP1, and p-CHK1 were significantly reduced in the combination group compared to the OXA alone group (Figure 6A, B). We also detected changes in mRNA levels using real-time PCR and obtained similar results (Figure 6C). Phosphorylated H_2AX histone (γ-H_2AX) is a marker of DNA double-strand breaks, and its quantification has become a standard method for quantifying DNA damage levels in experimental and clinical settings[26]. Western blotting showed that γ-H_2AX protein levels were robustly upregulated in the treated Hep3B and HepG2 cells (Figure 6A, B). This suggests that DNA damage levels further increased when DGD and OXA were used in combination. During cellular stress responses and DNA damage repair, p38 mitogen-activated protein kinase (p38 MAPK) and ATR signaling pathways interact and cooperate to maintain normal cellular physiological functions.

HM9_V6N3.indb 379 26-Sep-26 15:38:20

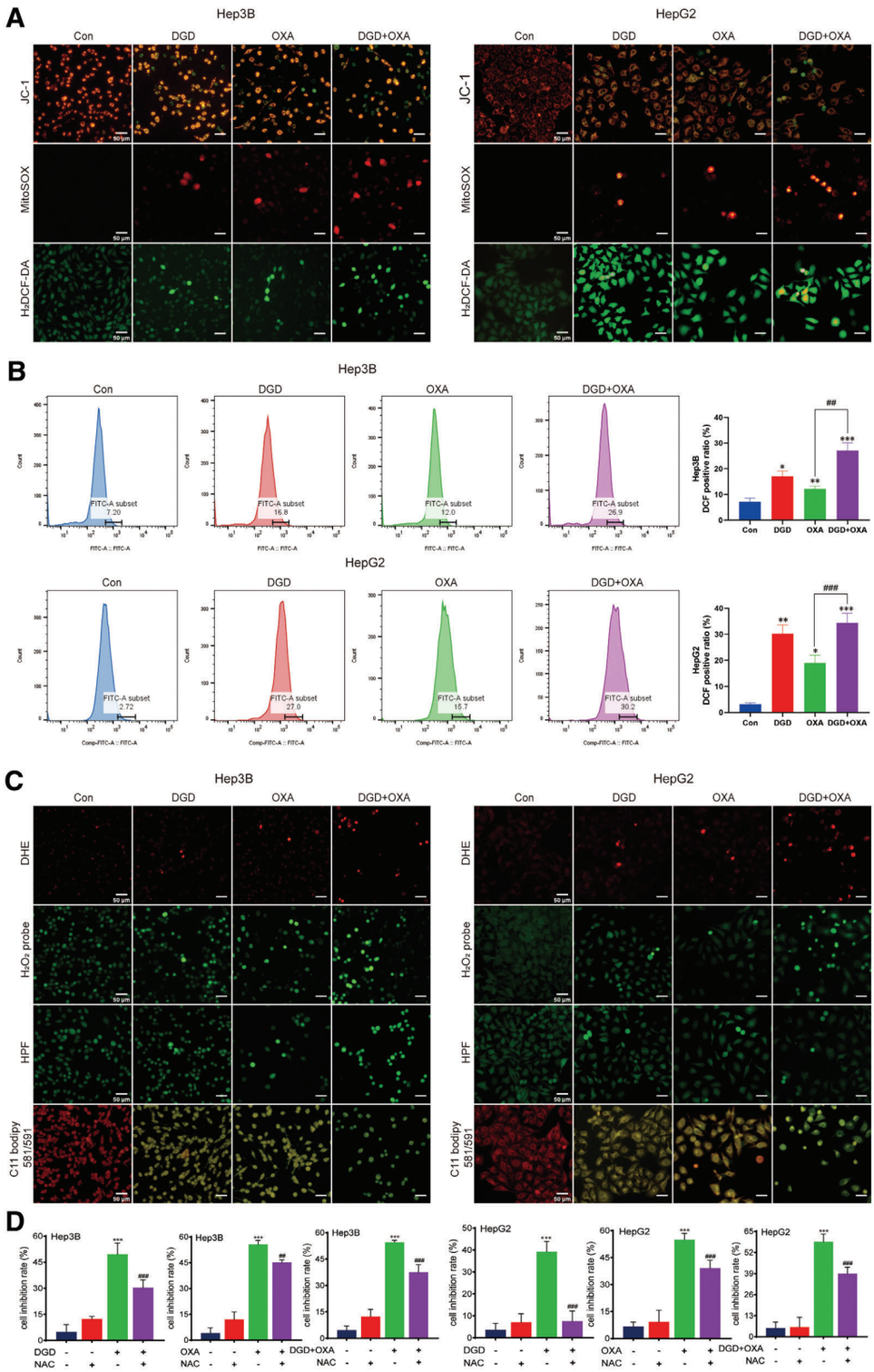


Figure 5. DGD enhances OXA-induced mitochondrial dysfunction and oxidative stress in liver cancer cells. (A) Fluorescence microscopic analysis of mitochondrial membrane potential, mitochondrial superoxide production, and ROS in Hep3B and HepG2 cells using fluorescent probes JC-1, MitoSOX™ Red, and H_2DCF-DA, respectively ($n = 3$). (B) Intracellular ROS levels were measured by H_2DCF-DA staining and flow cytometry ($n = 3$). The data are presented as mean ± SD of three independent experiments, $^{*}P < 0.05$, $^{**}P < 0.01$, $^{***}P < 0.001$ *vs*. control, $^{\#}P < 0.05$, $^{\#\#}P < 0.01$, $^{\#\#\#}P < 0.001$ *vs*. OXA group. (C) DHE, H_2O_2, HPF, and C11-BODIPY 581/591 staining were used to detect the effect of the combined drugs on oxidative stress in Hep3B and HepG2 cells ($n = 3$). Scale bar represents 50 μm. (D) Inhibitory effects of DGD, OXA, and the combination of DGD and OXA on Hep3B and HepG2 cells after NAC treatment ($n = 3$). The data are presented as the mean ± SD of three independent experiments. $^{*}P < 0.05$, $^{**}P < 0.01$, $^{***}P < 0.001$ *vs*. control group (A column), $^{\#}P < 0.05$, $^{\#\#}P < 0.01$, $^{\#\#\#}P < 0.001$ *vs*. DGD, OXA, or DGD + OXA group (C column). DGD: Daphnegiravone D; DHE: Dihydroethidium; H_2DCF-DA: Dichlorofluorescein diacetate; H_2O_2: Hydrogen peroxide; HPF: Hydroxyphenyl fluorescein; NAC: N-acetyl-L-cysteine; OXA: Oxaliplatin; ROS: Reactive oxygen species; SD: Standard deviation.

HM9_V6N3.indb 380 26-Sep-26 15:38:22

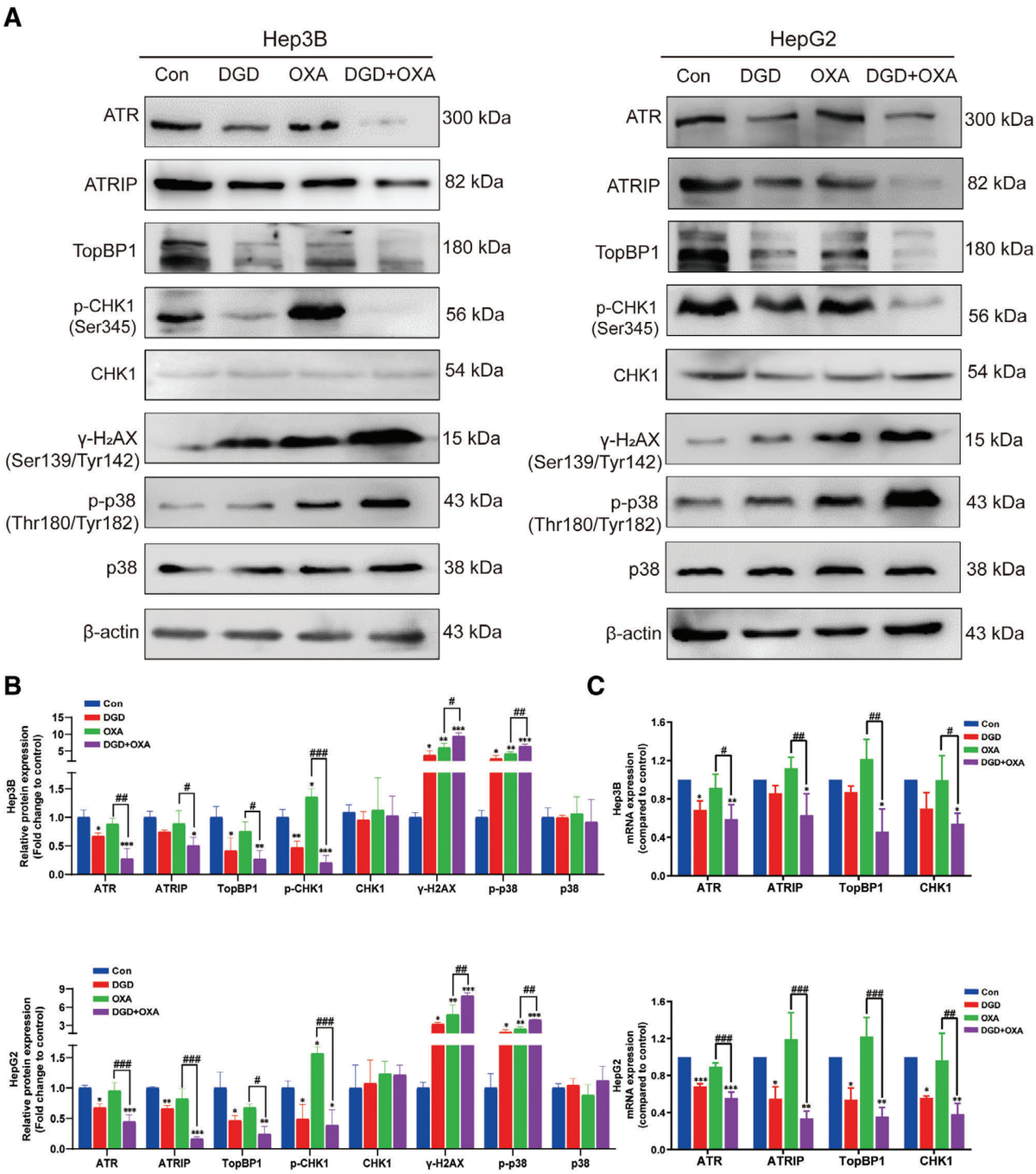


Figure 6. Effect of drug combination on the ATR signaling pathway. (A, B) The expression levels of ATR, ATRIP, TopBP1, p-CHK1, γ-H_2AX, p-p38, and p38 proteins were detected by western blotting (n = 3). (C) The effect of the combination therapy on the mRNA levels of ATR, ATRIP, TopBP1, and CHK1 was examined using RT-PCR (n = 3). All data are presented as the mean ± SD of three independent experiments, $^{*}P < 0.05$, $^{**}P < 0.01$, $^{***}P < 0.001$ *vs*. control, $^{\#}P < 0.05$, $^{\#\#}P < 0.01$, $^{\#\#\#}P < 0.001$ *vs*. OXA group. ATR: Ataxia telangiectasia and Rad3-related kinase; ATRIP: ATR-ATR-interacting protein; OXA: Oxaliplatin; RT-PCR: Reverse transcription-polymerase chain reaction; SD: Standard deviation.

Previous studies have demonstrated that activation of the p38 protein promoted DGD-induced apoptosis and oxidative stress[22,38]. Next, we examined the effects of the combination of DGD and OXA on the p38 pathway. As shown in Figure 6A and B, the activation of p38 (p-p38) was significantly upregulated after co-treatment with DGD and OXA. Taken together, These results suggest that suppression of ATR-related signaling may contribute, at least in part, to the enhanced sensitivity of liver cancer cells to OXA following DGD treatment.

Combined treatment with DGD and OXA was effective in treating liver cancer in vivo

Based on the above *in vitro* findings, the anti-tumor effects of DGD and OXA were examined in a Hep3B xenograft

HM9_V6N3.indb 381 26-Sep-26 15:38:23

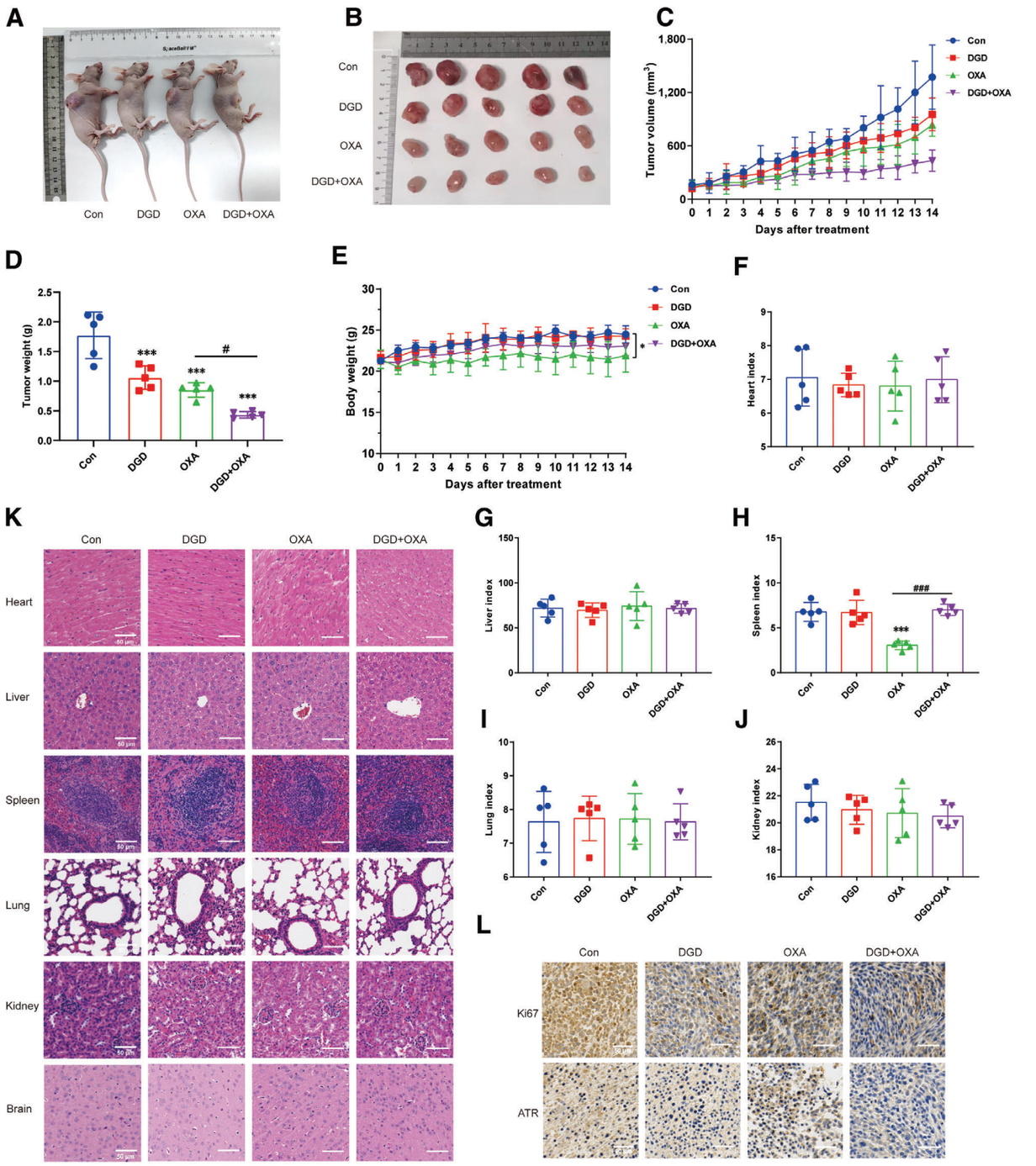


Figure 7. DGD enhances the *in vivo* efficacy of OXA. Hep3B cells were injected into nude mice, which were subsequently administered 5 mg/kg DGD and/or 5 mg/kg OXA (five mice per group). (A, B) Representative photographs of tumor-xenografted nude mice and tumors ($n = 5$). (C, D) Changes in tumor volume and weight were monitored ($n = 5$). (E) Body weight changes in tumor-bearing nude mice were monitored during the experiments ($n = 5$). (F–J) Index of the heart, liver, spleen, lung, and kidney obtained from Hep3B human xenograft mice after receiving different treatments ($n = 5$). (K) H&E staining was used to evaluate the major organs and brain of mice ($n = 5$). (L) Levels of Ki67 and ATR proteins in the indicated xenograft tumors were determined by immunohistochemical staining ($n = 5$). Scale bar represents 50 μm. All data are presented as means ± SD, $^{*}P < 0.05$, $^{**}P < 0.01$, $^{***}P < 0.001$ *vs*. control, $^{\#}P < 0.05$, $^{\#\#}P < 0.01$, $^{\#\#\#}P < 0.001$ *vs*. OXA group. ATR: Ataxia telangiectasia and Rad3-related kinase; DGD: Daphnegiravone D; H&E: Hematoxylin and eosin; OXA: Oxaliplatin; SD: Standard deviation.

model *in vivo*. As shown in Figure 7A–D, compared with tumor growth in the control group (glucose-treated group), DGD and OXA alone had a slight inhibitory effect on tumor growth, and the combination of OXA and DGD remarkably enhanced anti-tumor activity in mice compared with either monotherapy. Concurrently, the combined treatment showed no significant influence on body weight or the heart, liver, lung, spleen, kidney, or brain in nude mice, suggesting low or no systemic toxicity of the combination therapy (Figure 7E–K). Moreover,

HM9_V6N3.indb 382 26-Sep-26 15:38:24

a significant decrease in spleen index was observed in the OXA treatment group. However, the spleen index was upregulated after co-treatment with DGD and OXA compared to that in the OXA group (Figure 7H). This indicates that DGD moderated some of the side effects caused by OXA. Immunohistochemical analysis of the tumor tissues further verified that the combination of DGD and OXA inhibited the expression of ATR and Ki67, a cell proliferation-associated protein (Figure 7L). Taken together, these results indicate that DGD enhanced the antitumor efficacy of OXA *in vivo*, accompanied by reduced ATR expression in xenograft tumors.

Discussion

Liver cancer is a vascular tumor with a poor prognosis. Despite great progress in the treatment of liver cancer, combination chemotherapy remains the main treatment of choice for patients with unresectable metastatic or recurrent liver cancer[39]. It has been reported that icariin could exacerbate mitophagy and synergize with doxorubicin to induce cell death in liver cancer[40]. Silibinin has also been reported to enhance the growth-inhibitory effects of gefitinib and sorafenib on liver cancer cells[41–43]. Furthermore, Xie et al.[44] demonstrated that a combination of chrysophanol and VP-16 synergistically inhibited the viability of HepG2 cells. Moreover, it has been shown that flavonoids, isomorellin, and forbesione in combination with doxorubicin had a synergistic effect on growth inhibition and apoptosis induction in tumor cells[45].

The DNA damage response in tumor cells differs from that in normal cells, as it can limit the efficacy of cytotoxic chemotherapeutic agents and radiotherapy and promote DNA repair, which leads to tumor cell survival[46–47]. DNA damage response is regulated by two homologous protein kinases: ataxia telangiectasia–mutated (ATM) and Rad3-related (ATR)[48]. Therefore, targeting multiple DNA damage response pathways is an important strategy for improving the efficacy of DNA-damaging anticancer drugs[49]. Currently, eight ATR inhibitors have been evaluated in multiple early-stage clinical trials, and the majority of clinical trials with ATR inhibitors are combination studies, especially with platinum-based drugs, antimetabolites, and radiotherapy[50–51]. Studies have shown that ATR inhibition sensitizes cancer cells to chemotherapy, such as in pancreatic cancer (with gemcitabine) and lung cancer (with cisplatin, OXA, and gemcitabine)[52–54]. However, few studies have investigated the combined use of ATR inhibitors and chemotherapeutic drugs for liver cancer. Based on previous studies, we found that DGD may target and inhibit ATR[12]. The primary goal of the present study was to investigate whether DGD could potentiate the anti-tumor potential of OXA in liver cancer cells. In this study, we found that the combination of DGD and OXA was cytostatic and exhibited low cytotoxicity. Moreover, our results showed that DGD combined with OXA exhibited a synergistic inhibitory effect on tumor growth *in vivo*. We also found that DGD attenuated the side effects induced by OXA *in vivo*, which might improve patient compliance with OXA.

Activation of the ATR pathway is an extremely complex process. When DNA damage occurs, ATR and its functional partner ATRIP are recruited to the site of DNA damage, forming an active signaling complex[55]. Simultaneously, ATR recruits TopBP1, which stimulates the kinase activity of ATR and activates downstream factors such as CHK1 to promote genomic stability in response to DNA damage, cell cycle arrest, and stabilization of replication forks[56]. It is well known that OXA exerts an anti-tumor effect through its effects on DNA. However, it also induces a chemotherapy-protective signaling pathway, which may cause chemotherapy resistance. Iwata et al.[57] demonstrated that ATR is associated with OXA resistance. The addition of an ATR inhibitor reverses the activation of ATR and CHK1 by OXA, thereby synergistically inhibiting tumor cell proliferation. It has also been reported that OXA induces the activation of the ATR-CHK1 pathway but increases DNA damage when combined with an ATR inhibitor[58]. In our study, we found that combination treatment with DGD and OXA was associated with suppression of ATR-related signaling and CHK1 phosphorylation, similar to the results of other studies[59–60]. Furthermore, *in vivo*, DGD combined with OXA effectively reduced ATR activity in tumor tissues, which is consistent with the *in vitro* results. However, the lack of investigation on the level of related proteins such as p-CHK1 and γ-H2AX *in vivo* is a limitation of this study. Overall, isopentenyl flavones are expected to provide a new strategy for combination therapy by disrupting the damage response and reversing or preventing OXA resistance. However, the inhibitory effect of the DGD–OXA combination in OXA-resistant cell models remains unknown.

Platinum-based compounds have been reported to induce anti-tumor activity through oxidative stress and may contribute to ROS production[61–62]. Several recent studies have shown reduced anti-tumor effects when OXA is combined with NAC or a superoxide dismutase mimic, indicating that ROS generation plays a crucial role in OXA-treated cancer cells. In addition, it has been shown that piperlongumine in combination with OXA enhanced the inhibitory effect on colorectal cancer cells by inducing ROS-mediated mitochondrial dysfunction[61]. The present findings suggest that suppression of the DNA damage response and oxidative stress-associated mitochondrial dysfunction may represent complementary mechanisms contributing to the enhanced effect of DGD/OXA. Their precise hierarchical relationship remains unclear.

The MAPK signaling pathway plays a crucial role in various cellular responses[63]. P38, an important member of the MAPK family, is commonly associated with stress response, cell differentiation, and apoptotic cell death, and has been shown to play a vital role in the formation, development, and therapeutic response of tumors. It has been reported that OXA-induced DNA damage and oxidative stress ROS can simultaneously activate ATR and p38, and the functions of the two are antagonistic to each other. When ATR is inhibited, it promotes the pro-apoptotic effect of the P38 MAPK signaling pathway[63–65]. A previous study reported that rutin and OXA synergistically induce apoptosis in gastric cancer cells by activating the p38 signaling pathway[66]. In addition, recent studies have shown that some natural products, such as alantolactone and piperlongumine, can induce apoptotic cell death through activation

HM9_V6N3.indb 383 26-Sep-26 15:38:24

of the p38 signaling pathway *via* ROS accumulation, thereby enhancing the anti-tumor effects of OXA[67–68]. DGD upregulates the protein levels of p38. In a previous study, cell viability was clearly reduced after treatment with DGD, and this effect was abolished by SB203580 (a p38/MAPK-specific inhibitor)[12]. OXA also upregulated the protein level of p38, inhibiting liver cancer cells. Similarly, our data suggest that DGD combined with OXA may enhance anticancer effects by activating the p38 pathway.

Regarding the mechanism of toxicity, OXA often causes chronic neurotoxicity in patients, which is the main obstacle to its clinical application. This mechanism involves multiple pathological processes such as oxidative stress and neuroinflammation[69–70]. Isopentenyl flavonoids have shown great potential in preclinical studies, as they exert neuroprotective effects by targeting these key pathways[71]. In addition, DGD was isolated from *D. giraldii* Nitsche, the original plant of *ZuShiMa*, which has been used to treat traumatic injuries and has obvious anti-inflammatory effects. Therefore, we speculated that DGD protects normal cells through anti-inflammatory mechanisms. The combined use of OXA and DGD reduced the effective dose of OXA, thereby alleviating its toxicity.

Limitation

Despite compelling evidence that DGD improved the anti-tumor effect of the chemotherapeutic drug OXA on liver cancer, our study has limitations. First, drug resistance is a major cause of treatment failure. Current evidence supports chemosensitization, not reversal of established resistance. The inhibitory effect of the DGD–OXA combination should be evaluated in OXA–resistant hepatocellular carcinoma cell models. In addition, pharmacokinetic and pharmacodynamic studies are needed to study the mechanism in vivo, optimize treatment plans, and ensure medication safety. Therefore, future studies should focus on addressing these questions.

Conclusion

In summary, our data demonstrated that DGD greatly enhanced the anti-tumor effect of the chemotherapeutic drug OXA on liver cancer both *in vitro* and *in vivo*. This synergism probably resulted from the fact that DGD suppressed the ATR-CHK1 signaling pathway by inhibiting the activation of the ATR protein, which in turn restrained the DNA damage response process induced by OXA. DGD also potentiated the inhibitory effects of OXA on liver cancer cells by increasing mitochondrial functional impairment and oxidative stress. Taken together, the current study supports the concept that an OXA-based regimen in combination with DGD can result in a more powerful anti-liver cancer effect, revealing a promising new approach for the treatment of liver cancer. This warrants further evaluation in future clinical settings.

Conflict of interest statement

The authors declare no conflict of interest.

Funding

This research work was supported by the National Natural Science Foundation of China (81973528, 82273821), LiaoNing Revitalization Talents Program (XLYC2503156), Youth Innovation Team Scientific Research Project of Liaoning Provincial Department of Education (LT222410163052), Natural Science Foundation of Liaoning province (2022-MS-244), Young Elite Scientists Sponsorship Program by CACM (2023-QNRC2-B24), Innovation Team and Talents Cultivation Program of National Administration of Traditional Chinese Medicine (ZYYCXTD-D-202208), Plan of Shenyang Young and Middle-aged Science and Technology Innovation Talents Support (RC210451), the Scientific Research Fund Project of Liaoning Provincial Department of Education (LJKZ0907), China Postdoctoral Science Foundation (2019M661135), Song Shaojiang Expert Workstation of Yunnan Province (202305 AF150030), the Outstanding and Excellent Youth Talent Support Program of Shenyang Pharmaceutical University (ZQ202201, YQ202104), the Liaoning Revitalization Talents Program (No. XLYC2002066), and Science and Technology Planning Project of Liaoning Province (2021JH1/10400049).

Author contributions

Yu-Jue Wang and Jiao-Yang Hou performed the experiments, analyzed the data, and drafted and revised the manuscript. Xin-Ye Wang and Hong-Fei Chen contributed to the discussion and revision of the manuscript. Shuang Qiu, Qing-Bo Liu, and Xiao-Xiao Huang provided compounds used in this study. Guo-Dong Yao and Shao-Jiang Song conceived and designed this study, wrote and revised the manuscript, and conducted the project administration. Qing-Bo Liu, Guo-Dong Yao, and Shao-Jiang Song acquired the funding grants.

Ethical approval of studies and informed consent

The animal procedures were approved by Shenyang Pharmaceutical University (registration number: SYXK (Liao) 2021-0009, ethical approval number: SYPU-IACUC-S2022-10.19-101) and followed the Guide for the Care and Use of Laboratory Animals.

Acknowledgments

None.

Data availability statement

All data generated or analyzed in this study are included in this published article; further inquiries can be directed to the corresponding authors.

Declaration of generative AI in scientific writing

The conception and writing of this article were carried out collaboratively by all authors. Artificial intelligence was utilized exclusively for refining sentence coherence and amending punctuation. All citations in this manuscript were manually searched for and incorporated.

HM9_V6N3.indb 384 26-Sep-26 15:38:24

After utilizing the aforementioned tools/services, the authors thoroughly reviewed and revised the content and take full responsibility for the entirety of this publication.

References

[1] Li Q, Xia C, Li H, et al. Disparities in 36 cancers across 185 countries: secondary analysis of global cancer statistics. *Front Med* 2024;18(5):911–920.
[2] Zhang Y, Lu L, Chen M, et al. Identification and validation of ATP6V1G1-regulated phosphorylated proteins in hepatocellular carcinoma. *PLoS One* 2024;19(12):e0310037.
[3] Zhang Y, Zhou X, Zhai J, et al. The role of SIRT1 in the development of gastrointestinal tumors. *Front Cell Dev Biol* 2025;13:1606530.
[4] Hsieh CC, Hsu SH, Lin CY, et al. CHK2 activation contributes to the development of oxaliplatin resistance in colorectal cancer. *Br J Cancer* 2022;127(9):1615–1628.
[5] Liu S, Bu X, Kan A, et al. SP1-induced lncRNA DUBR promotes stemness and oxaliplatin resistance of hepatocellular carcinoma *via* E2F1-CIP2A feedback. *Cancer Lett* 2022;528:16–30.
[6] Li W, Zou L, Huang S, et al. The anticancer activity of bile acids in drug discovery and development. *Front Pharmacol* 2024;15:1362382.
[7] Al-Otaibi WA, AlMotwaa SM. Oxaliplatin-loaded nanoemulsion containing Teucrium polium L. essential oil induces apoptosis in colon cancer cell lines through ROS-mediated pathway. *Drug Deliv* 2022;29(1):2190–2205.
[8] Khan H, Ullah H, Martorell M, et al. Flavonoids nanoparticles in cancer: treatment, prevention and clinical prospects. *Semin Cancer Biol* 2021;69:200–211.
[9] Li S, Yuan S, Zhao Q, et al. Quercetin enhances chemotherapeutic effect of doxorubicin against human breast cancer cells while reducing toxic side effects of it. *Biomed Pharmacother* 2018;100:441–447.
[10] Fernández J, Silván B, Entrialgo-Cadierno R, et al. Antiproliferative and palliative activity of flavonoids in colorectal cancer. *Biomed Pharmacother* 2021;143:112241.
[11] Rajendran P, Rengarajan T, Nandakumar N, et al. Kaempferol, a potential cytostatic and cure for inflammatory disorders. *Eur J Med Chem* 2014;86:103–112.
[12] Shang XY, Yu XQ, Yao GD, et al. Daphnegiravone D from Daphne giraldii induces cell death by targeting ATR in Hep3B cells. *Bioorg Chem* 2021;110:104802.
[13] Prasad CB, Oo A, Liu Y, et al. The thioredoxin system determines CHK1 inhibitor sensitivity *via* redox-mediated regulation of ribonucleotide reductase activity. *Nat Commun* 2024;15:4667.
[14] Zhang Y, Chen Y, Huang W, et al. NPAS2 dampens chemosensitivity of lung adenocarcinoma cells by enhancing DNA damage repair. *Cell Death Dis* 2024;15(1):101.
[15] Xie D, Jiang B, Wang S, et al. The mechanism and clinical application of DNA damage repair inhibitors combined with immune checkpoint inhibitors in the treatment of urologic cancer. *Front Cell Dev Biol* 2023;11:1200466.
[16] Ngoi NYL, Peng G, Yap TA. A tale of two checkpoints: ATR inhibition and PD-(L)1 blockade. *Annu Rev Med* 2022;73:231–250.
[17] Groelly FJ, Fawkes M, Dagg RA, et al. Targeting DNA damage response pathways in cancer. *Nat Rev Cancer* 2023;23(2):78–94.
[18] Zhu H, Tian Y, Chen H, et al. Targeting DNA damage response pathways in tumor drug resistance: mechanisms, clinical implications, and future directions. *Drug Resist Updat* 2025;83:101287.
[19] Derby SJ, Dutton L, Strathdee KE, et al. Inhibition of ATR opposes glioblastoma invasion through disruption of cytoskeletal networks and integrin internalization *via* macropinocytosis. *Neuro Oncol* 2024;26(4):625–639.
[20] Mei L, Zhang J, He K, et al. Ataxia telangiectasia and Rad3-related inhibitors and cancer therapy: where we stand. *J Hematol Oncol* 2019;12(1):43.
[21] Revythis A, Limbu A, Mikropoulos C, et al. Recent insights into PARP and immuno-checkpoint inhibitors in epithelial ovarian cancer. *Int J Environ Res Public Health* 2022;19(14):8577.
[22] Wang D, Sun Q, Wu J, et al. A new prenylated flavonoid induces G0/G1 arrest and apoptosis through p38/JNK MAPK pathways in human hepatocellular carcinoma cells. *Sci Rep* 2017;7(1):5736.
[23] Zheng S, Wang W, Aldahdooh J, et al. SynergyFinder plus: toward better interpretation and annotation of drug combination screening datasets. *Genomics Proteomics Bioinformatics* 2022;20(3):587–596.
[24] Zhang Q, Zhou Y, Feng X, et al. Low-dose orlistat promotes the therapeutic effect of oxaliplatin in colorectal cancer. *Biomed Pharmacother* 2022;153:113426.
[25] Gorecki L, Andrs M, Rezacova M, et al. Discovery of ATR kinase inhibitor berzosertib (VX-970, M6620): clinical candidate for cancer therapy. *Pharmacol Ther* 2020;210:107518.
[26] Lecona E, Fernandez-Capetillo O. Targeting ATR in cancer. *Nat Rev Cancer* 2018;18(9):586–595.
[27] Gralewska P, Gajek A, Marczak A, et al. PARP inhibition increases the reliance on ATR/CHK1 checkpoint signaling leading to synthetic lethality-an alternative treatment strategy for epithelial ovarian cancer cells independent from HR effectiveness. *Int J Mol Sci* 2020;21(24):9715.
[28] Qu H, Shi X, Xu Y, et al. Mechanism of Musashi2 affecting radiosensitivity of lung cancer by modulating DNA damage repair. *MedComm (2020)* 2024;5(5):e548.
[29] Sun Y, Wang J, Ma Y, et al. Radiation induces NORAD expression to promote ESCC radiotherapy resistance *via* EEPD1/ATR/Chk1 signalling and by inhibiting pri-miR-199a1 processing and the exosomal transfer of miR-199a-5p. *J Exp Clin Cancer Res* 2021;40(1):306.
[30] Fernandez A, Artola M, Leon S, et al. Cancer vulnerabilities through targeting the ATR/Chk1 and ATM/Chk2 axes in the context of DNA damage. *Cells* 2025;14(10):748.
[31] Foote KM, Lau A, Nissink JWM. Drugging ATR: progress in the development of specific inhibitors for the treatment of cancer. *Future Med Chem* 2015;7(7):873–891.
[32] Segeren HA, Wierenga KA, Riemers FM, et al. Stochastic variation in the FOXM1 transcription program mediates replication stress tolerance. *Mol Oncol* 2025;19(6):1633–1650.
[33] Khalilzadeh B, Shadjou N, Eskandani M, et al. A reliable self-assembled peptide based electrochemical biosensor for detection of caspase-3 activity and apoptosis. *RSC Adv* 2015;5(72):58316–58326.
[34] Han X, Peng B, Xiao BB, et al. Synthesis and evaluation of chalcone analogues containing a 4-oxoquinazolin-2-yl group as potential anti-tumor agents. *Eur J Med Chem* 2019;162:586–601.
[35] Zhang X, Han J, Xu Y, et al. TSPO deficiency exacerbates GSDMD-mediated macrophage pyroptosis in inflammatory bowel disease. *Cells* 2022;11(5):856.
[36] Xing YJ, Liu BH, Wan SJ, et al. A SGLT2 inhibitor dapagliflozin alleviates diabetic cardiomyopathy by suppressing high glucose-induced oxidative stress *in vivo* and *in vitro*. *Front Pharmacol* 2021;12:708177.
[37] Xiang K, Wang B, Wang L, et al. Oxidative stress, oxidative damage, and cell apoptosis: toxicity induced by arecoline in Caenorhabditis elegans and screening of mitigating agents. *Toxins (Basel)* 2024;16(8):352.
[38] Shang XY, Chen JJ, Song XY, et al. Daphnegiravone D from Daphne giraldii Nitsche induces p38-dependent apoptosis *via* oxidative and nitrosative stress in hepatocellular carcinoma cells. *Biomed Pharmacother* 2018;107:1426–1433.
[39] Zhang Y, Li Q, Wang J, et al. Polysaccharide from Lentinus edodes combined with oxaliplatin possesses the synergy and attenuation effect in hepatocellular carcinoma. *Cancer Lett* 2016;377(2):117–125.
[40] Yu Z, Guo J, Hu M, et al. Icaritin exacerbates mitophagy and synergizes with doxorubicin to induce immunogenic cell death in hepatocellular carcinoma. *ACS Nano* 2020;14(4):4816–4828.
[41] Mao J, Yang H, Cui T, et al. Combined treatment with sorafenib and silibinin synergistically targets both HCC cells and cancer stem cells by enhanced inhibition of the phosphorylation of STAT3/ERK/AKT. *Eur J Pharmacol* 2018;832:39–49.
[42] Gu HR, Park SC, Choi SJ, et al. Combined treatment with silibinin and either sorafenib or gefitinib enhances their growth-inhibiting effects in hepatocellular carcinoma cells. *Clin Mol Hepatol* 2015;21(1):49–59.
[43] Ray PP, Islam MA, Islam MS, et al. A comprehensive evaluation of the therapeutic potential of silibinin: a ray of hope in cancer treatment. *Front Pharmacol* 2024;15:1349745.
[44] Xie Y, Zhang L, Li YY, et al. Chrysophanol localizes in mitochondria to promote cell death through upregulation of mitochondrial cyclophilin D in HepG2 cells. *Chin Herb Med* 2021;13(2):221–227.
[45] Phang YL, Zheng C, Xu H. Structural diversity and biological activities of caged Garcinia xanthones: recent updates. *Acta Materia Medica* 2022;1(1):72–95.
[46] Jackson SP, Bartek J. The DNA-damage response in human biology and disease. *Nature* 2009;461(7267):1071–1078.

HM9_V6N3.indb 385 26-Sep-26 15:38:25

[47] Zhang L, Zhuang Y, Tu G, et al. Positive feedback regulation of Poly(ADP-ribose) polymerase 1 and the DNA-PK catalytic subunit affects the sensitivity of nasopharyngeal carcinoma to etoposide. *ACS Omega* 2022;7(3):2571–2582.
[48] Harper JW, Elledge SJ. The DNA damage response: ten years after. *Mol Cell* 2007;28(5):739–745.
[49] Fokas E, Prevo R, Hammond EM, et al. Targeting ATR in DNA damage response and cancer therapeutics. *Cancer Treat Rev* 2014;40(1):109–117.
[50] Stewart J, Krastev DB, Brough R, et al. PPP2R1A mutations cause ATR inhibitor sensitivity in ovarian clear cell carcinoma. *Oncogene* 2025;44(9):618–629.
[51] Smith HL, Southgate H, Tweddle DA, et al. DNA damage checkpoint kinases in cancer. *Expert Rev Mol Med* 2020;22:e2.
[52] Hall AB, Newsome D, Wang Y, et al. Potentiation of tumor responses to DNA damaging therapy by the selective ATR inhibitor VX-970. *Oncotarget* 2014;5(14):5674–5685.
[53] Fauvre A, Ursino C, Garambois V, et al. Oxaliplatin, ATR inhibitor and anti-PD-1 antibody combination therapy controls colon carcinoma growth, induces local and systemic changes in the immune compartment, and protects against tumor rechallenge in mice. *J ImmunoTher Cancer* 2025;13(3):e010791.
[54] Shapiro GI, Wesolowski R, Devoe C, et al. Phase 1 study of the ATR inhibitor berzosertib in combination with cisplatin in patients with advanced solid tumours. *Br J Cancer* 2021;125(4):520–527.
[55] Wu CS, Ouyang J, Mori E, et al. SUMOylation of ATRIP potentiates DNA damage signaling by boosting multiple protein interactions in the ATR pathway. *Genes Dev* 2014;28(13):1472–1484.
[56] Liu S, Shiotani B, Lahiri M, et al. ATR autophosphorylation as a molecular switch for checkpoint activation. *Mol Cell* 2011;43(2):192–202.
[57] Iwata T, Uchino T, Koyama A, et al. The G2 checkpoint inhibitor CBP-93872 increases the sensitivity of colorectal and pancreatic cancer cells to chemotherapy. *PLoS One* 2017;12(5):e0178221.
[58] Perego P, Zunino F, Carenini N, et al. Sensitivity to cisplatin and platinum-containing compounds of Schizosaccharomyces pombe rad mutants. *Mol Pharmacol* 1998;54(1):213–219.
[59] Zhang Y, Xie C, Li A, et al. PKI-587 enhances chemosensitivity of oxaliplatin in hepatocellular carcinoma through suppressing DNA damage repair pathway (NHEJ and HR) and PI3K/AKT/mTOR pathway. *Am J Transl Res* 2019;11(8):5134–5149.
[60] Combès E, Andrade AF, Tosi D, et al. Inhibition of ataxia-telangiectasia mutated and RAD3-related (ATR) overcomes oxaliplatin resistance and promotes antitumor immunity in colorectal cancer. *Cancer Res* 2019;79(11):2933–2946.
[61] Chen W, Lian W, Yuan Y, et al. The synergistic effects of oxaliplatin and piperlongumine on colorectal cancer are mediated by oxidative stress. *Cell Death Dis* 2019;10(8):600.
[62] Lee J, Jang CH, Kim Y, et al. Quercetin-induced glutathione depletion sensitizes colorectal cancer cells to oxaliplatin. *Foods* 2023;12(8):1733.
[63] Wang J, Wei B, Thakur K, et al. Transcriptome analysis reveals the anti-cancerous mechanism of licochalcone A on human hepatoma cell HepG2. *Front Nutr* 2021;8:807574.
[64] Guo YJ, Pan WW, Liu SB, et al. ERK/MAPK signalling pathway and tumorigenesis. *Exp Ther Med* 2020;19(3):1997–2007.
[65] Gräb J, Rybniker J. The expanding role of p38 mitogen-activated protein kinase in programmed host cell death. *Microbiol Insights* 2019;12:1178636119864594.
[66] Li Q, Ren L, Zhang Y, et al. P38 signal transduction pathway has more cofactors on apoptosis of SGC-7901 gastric cancer cells induced by combination of rutin and oxaliplatin. *Biomed Res Int* 2019;2019:6407210.
[67] Cao P, Xia Y, He W, et al. Enhancement of oxaliplatin-induced colon cancer cell apoptosis by alantolactone, a natural product inducer of ROS. *Int J Biol Sci* 2019;15(8):1676–1684.
[68] Zhang P, Shi L, Zhang T, et al. Piperlongumine potentiates the antitumor efficacy of oxaliplatin through ROS induction in gastric cancer cells. *Cell Oncol (Dordr)* 2019;42(6):847–860.
[69] Misset JL. Oxaliplatin in practice. *Br J Cancer* 1998;77(Suppl 4):4–7.
[70] Wei G, Gu Z, Gu J, et al. Platinum accumulation in oxaliplatin-induced peripheral neuropathy. *J Peripher Nerv Syst* 2021;26(1):35–42.
[71] Santi MD, Arredondo F, Carvalho D, et al. Neuroprotective effects of prenylated flavanones isolated from Dalea species, in vitro and in silico studies. *Eur J Med Chem* 2020;206:112718.

HM9_V6N3.indb 386 26-Sep-26 15:38:25